

# Large-Scale Synthesis and Applications of Hafnium-Tantalum Carbides

Alexander G. Kvashnin,\* Dmitry S. Nikitin,\* Ivan I. Shanenkov, Ilia V. Chepkasov, Yulia A. Kvashnina, Artur Nassyrbayev, Alexander A. Sivkov, Zhanar Bolatova, and Alexander Ya. Pak

Comprehensive theoretical and experimental studies are performed to discover a new way of synthesis of Hf–Ta–C coatings. Here, an evolutionary search for stable crystal structures in the ternary Hf–Ta–C system with subsequent selective large-scale experimental synthesis of coatings using a unique plasma dynamic experimental setup is performed. Optimization of the experimental process allows us to perform selective synthesis of coatings made of hafnium–tantalum carbides with predefined stoichiometry, crystal structure, and properties. Along with more than 70 compounds, the Hf–Ta–C system belongs to ternary and quaternary carbides of group IV and V transition metals, and this study opens the door to synthesis of a large number of functional coatings composed of other carbides including high-entropy carbides.

## 1. Introduction

Carbides of transition metals usually considered as industrially important materials as they display ultrahigh melting temperatures,<sup>[1,2]</sup> high hardness, and wear resistance.<sup>[3,4]</sup> Binary hafnium and tantalum carbides are the most refractory with highest melting temperature close to 4000 °C.<sup>[5]</sup> Both HfC and TaC exhibit a B1 NaCl-type crystal structure possessing similar physical and

chemical properties. Thus, investigations, synthesis, and applications of potential mixed hafnium-tantalum carbides have rapidly grown practical interest due to possibility to increase the melting point. As was shown by Castle et al.<sup>[6]</sup> the main driving factor for diffusion of metallic species is the formation of nearest-neighbor vacancy that can be occupied by diffusing atoms. Indeed, vacancy formation energies of host metallic atom in HfC is 2.5 times higher than that in TaC (9.3 and 3.5 eV, respectively<sup>[7]</sup>). This explains the perfect mixing of hafnium and tantalum atoms within the NaCl-type structure leading to formation of ternary Hf–Ta–C compounds.

It is known that most of ternary hafnium–tantalum carbides form phases with stoichiometry  $Ta_xHf_{1-x}C$  which are the homogeneous HfC–TaC solid solutions with various compositions.<sup>[8–10]</sup> Among these compounds the most studied one is  $Ta_4HfC_5$  ( $Ta_{0.80}Hf_{0.20}C$ ) displaying the highest experimentally observed melting temperature of ≈4200 K.<sup>[11,12]</sup> More recent experiments have determined the melting temperature of 4232 K for a composition of  $HfC_{0.98}$ .<sup>[13]</sup>

Formation of ternary compound as a solid solution of binary ones also leads to improvement in mechanical properties. Mechanical properties of  $Ta_{0.80}Hf_{0.20}C$  were studied by Ghafari et al.<sup>[14]</sup> where the hardness of synthesized by spark plasma sample was found to be between 15 and 18.2 GPa. It was also shown in Ref. [13,14] that variation of hardness of Hf–Ta–C from 15 to 21 GPa caused by the differences in fabrication method leading to uncontrollable porosity of products.

Detailed study of formation of new Hf–Ta–C compounds along with experimental synthesis and examination of deformation slips was reported by Smith et al.<sup>[15]</sup> Fixed-composition evolutionary search allowed the prediction of five stable ternary  $Ta_xHf_{1-x}C$  solid solutions, namely  $Hf_5TaC_6$  ( $Hf_{0.83}Ta_{0.17}C$ ),  $Hf_3TaC_4$  ( $Hf_{0.75}Ta_{0.25}C$ ),  $HfTaC_2$  ( $Hf_{0.50}Ta_{0.50}C$ ),  $HfTa_3C_4$  ( $Hf_{0.25}Ta_{0.75}C$ ), and  $HfTa_5C_8$  ( $Hf_{0.13}Ta_{0.87}C$ ).<sup>[15]</sup> These compounds were synthesized by using spark plasma sintering (SPS) technique and Vickers hardness were measured to be in a range from 18 to 30 GPa.

Another recent theoretical work reported about computational prediction of stable structures in Hf–Ta–C system by using co-evolutionary algorithm COPEX.<sup>[16]</sup> A number of stable structures were predicted to be stable at 0 K where 10 out of the 14 stable belong to HfC–TaC solid solutions, while other four

A. G. Kvashnin, I. V. Chepkasov  
 Skolkovo Institute of Science and Technology  
 Skolkovo Innovation Center  
 Bolshoy Boulevard 30, bld. 1, Moscow 121205, Russia  
 E-mail: a.kvashnin@skoltech.ru

D. S. Nikitin, I. I. Shanenkov, A. Nassyrbayev, A. A. Sivkov,  
 Z. Bolatova, A. Ya. Pak  
 National Research Tomsk Polytechnic University  
 30 Lenin Avenue, Tomsk 634050, Russia  
 E-mail: nikitindmsr@yandex.ru

I. I. Shanenkov  
 University of Tyumen  
 6 Volodarskogo st., Tyumen 625003, Russia

Yu. A. Kvashnina  
 Pirogov Russian National Research Medical University  
 1 Ostrovityanova St., Moscow 117997, Russia

A. A. Sivkov  
 College of Communication Engineering  
 Jilin University  
 Changchun 130023, PR China

 The ORCID identification number(s) for the author(s) of this article can be found under <https://doi.org/10.1002/adfm.202206289>.

DOI: [10.1002/adfm.202206289](https://doi.org/10.1002/adfm.202206289)

were described as vacancy-ordered derivatives of the rocksalt structure.

However, none of the mentioned experimental studies devoted to complex investigation and synthesis of nonstoichiometric Hf–Ta–C compounds, which do not belong to class of HfC–TaC solid solutions. The available data about stable structures in the Hf–Ta–C system includes only the rocksalt crystal structure type, with no information regarding other types or nonstoichiometric structures.

It is crucially important that usually the synthesis of refractory carbides of transition metals (including high-entropy carbides) is performed in vacuum using various sintering techniques, like spark plasma sintering (SPS).<sup>[6,8,10,14,15,17,18]</sup> Less common synthesis methods include hot isostatic pressing,<sup>[15]</sup> and other techniques,<sup>[19–22]</sup> but all mentioned techniques require vacuum for the synthesis of high-quality carbide materials and thus are expensive and resource-consuming.

Here we demonstrate a unique, inexpensive and efficient plasma dynamic technique to synthesize high-quality ternary Hf–Ta–C compounds both as powders and coatings that can be easily applied to various substrates. Prior to the experimental synthesis, we performed a variable-composition computational prediction of a new stable crystal structures in the Hf–Ta–C

system with subsequent investigation of temperature and dynamic stability.

## 2. Results and Discussions

### 2.1. Computational Search

Refractory metal carbides have a cubic B1 rocksalt crystal structure with  $Fm\bar{3}m$  (no. 225) space group. Studied ternary metal carbides contain two refractory metals in the composition and are also based on the rocksalt structure type. Considering the global symmetry of the rocksalt structure, an assumption can be made that metal atoms in ternary carbides occupy the Wyckoff position 4a, whereas carbon usually occupies the Wyckoff position 4b. However, the possibility of formation of carbide having nonstoichiometric crystal structures with deficient or excessive carbon atoms remains an open question.

To solve this issue, we used USPEX evolutionary algorithm to predict stable crystal structures in the Hf–Ta–C system. The calculated ternary phase diagram at zero pressure and 0 K (Figure 1a) shows many various ternary compounds that can be stable at these conditions. Thermodynamically stable phase has

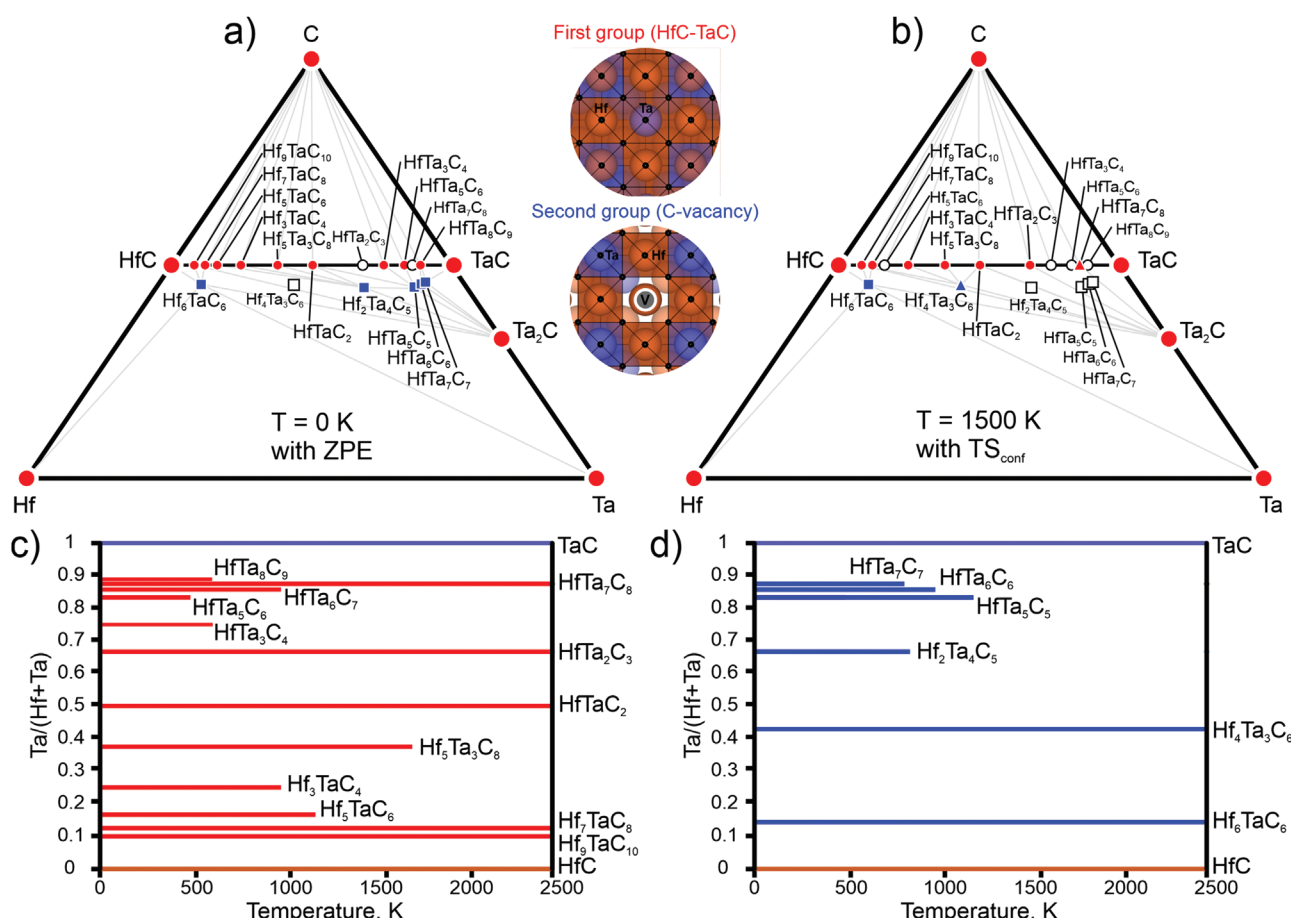


**Figure 1.** Ternary phase diagram of the Hf–Ta–C system at a) 0 and b) 1500 K. Thermodynamically stable and metastable compounds are shown in red/blue and white, respectively. Triangles denote compounds stabilized by the configurational entropy contribution. Composition–temperature phase diagrams calculated for the compounds of the c) first and d) second groups (the difference in their crystal structures is shown in the inset, where V denotes carbon vacancy).

lower energy (or Gibbs free energy at finite temperature) than any phase of the same composition. The predicted ternary compounds can be divided into two groups: the first one is formed by the  $\text{Hf}_x\text{Ta}_y\text{C}_z$  structures where  $x + y = z$  (shown by circles in Figure 1a); the structures where  $x + y \neq z$  belong to the second group (squares in Figure 1a). At 0 K, the first group has nine stable compounds, which can be considered as  $\text{HfC}-\text{TaC}$  solid solutions. The crystal structures with coordinates and lattice parameters are presented in Table S4 (Supporting Information). All these compounds have the rocksalt structure type and differ from each other by the amount of tantalum with respect to hafnium. The second group of structures contains five stable and one metastable ( $\text{Hf}_4\text{Ta}_3\text{C}_6$ ) compound at 0 K. These compounds also belong to the rocksalt structure type but have a deficiency of carbon atoms in the Wyckoff position 4b of the NaCl lattice (Figure 1 inset).

We calculated the phonon densities of states (DOS) for 69 predicted compounds that lie above the convex hull by 20 meV per atom to estimate their stability at finite temperatures. The obtained data indicates the dynamical stability of all predicted phases where none of imaginary modes can be observed. Integration over the phonon DOS allowed us to calculate the zero-point energy and vibrational Helmholtz free energy for all studied compounds and construct the convex hull at finite temperatures.

The convex hull (Maxwell construction) calculated at 1500 K shows the stabilization of many  $\text{Hf}_x\text{Ta}_y\text{C}_{x+y}$  structures, mainly  $\text{HfC}-\text{TaC}$  solid solutions (Figure 1b). To calculate the phase diagram at high temperatures, we examined the configurational entropy considering that all possible configurations of Hf and Ta in the structure within each composition have similar energies. The configurational entropy of each ternary compound was estimated using Boltzmann's entropy formula  $S_{\text{conf}} = k_B \ln W$ , where  $W$  is the number of possible configurations within one structure, i.e., the number of permutations of Hf and Ta atoms in the lattice. We used the approximate formula that gave us the upper limit for the configurational entropy of a  $\text{Hf}_x\text{Ta}_{1-x}\text{C}$  solid solution:

$$S_{\text{conf}} = k_B(x \ln x + (1-x) \ln (1-x)) \quad (1)$$

For structures from the second group, which have empty carbon sites, we consider the composition  $\text{Hf}_x\text{Ta}_{1-x}\text{C}_y\text{X}_{1-y}$ , where X is the carbon vacancy. In this case, additional configurations of carbon vacancies can be estimated using the formula

$$S_{\text{conf}} = k_B(x \ln x + (1-x) \ln (1-x) + y \ln y + (1-y) \ln (1-y)) \quad (2)$$

Configurational entropy may significantly expand the stability ranges of ternary compounds at high temperatures.

The stability of the predicted compounds at different temperatures is summarized in the composition–temperature phase diagrams (Figure 1c,d). In the first group (Figure 1c), only five structures are stable up to 2500 K ( $\text{HfTa}_7\text{C}_8$ ,  $\text{HfTa}_2\text{C}_3$ ,  $\text{HfTaC}_2$ ,  $\text{Hf}_7\text{TaC}_8$ , and  $\text{Hf}_9\text{TaC}_{10}$ ), whereas only three structures from the second group,  $\text{Hf}_4\text{Ta}_3\text{C}_6$ ,  $\text{Hf}_5\text{Ta}_3\text{C}_8$ , and  $\text{Hf}_6\text{TaC}_6$ , are stable at high temperatures (Figure 1d). For further theoretical and experimental investigations, we selected eight predicted compounds (six from the first group and two from the

second group):  $\text{Hf}_9\text{TaC}_{10}$ ,  $\text{Hf}_7\text{TaC}_8$ ,  $\text{Hf}_6\text{TaC}_6$ ,  $\text{Hf}_3\text{TaC}_4$ ,  $\text{Hf}_4\text{Ta}_3\text{C}_6$ ,  $\text{HfTaC}_2$ ,  $\text{HfTa}_2\text{C}_3$ , and  $\text{HfTa}_7\text{C}_8$ . We also added two individual carbides,  $\text{HfC}$  and  $\text{TaC}$ , as boundary compositions for the experimental synthesis, for a total of 10 structures.

The calculated phonon densities of states for 10 selected  $\text{Hf}-\text{Ta}-\text{C}$  compounds that were synthesized experimentally (see below) are shown in Figure S4 (Supporting Information). The calculated contributions to the Helmholtz free energy of these compounds are presented in Table S5 (Supporting Information); we studied their mechanical properties, which are listed in Table S6 (Supporting Information).

## 2.2. Experimental Synthesis

The comprehensive computational predictions of new non-stoichiometric compounds in the  $\text{Hf}-\text{Ta}-\text{C}$  system revealed important information about the compositions of new compounds for a targeted synthesis. For ten selected compositions, including  $\text{HfC}$  and  $\text{TaC}$ , we defined the initial mass ratio of precursors for each desired composition as listed in Table S1 (Supporting Information). Using the plasma dynamic synthesis, we conducted a series of successful experiments, obtaining ten different powder samples of  $\text{Hf}_x\text{Ta}_y\text{C}_z$ . The elemental composition of the synthesized material was determined using the EDS method in combination with the scanning electron microscopy. The results of the SEM and EDS analysis for the boundary compositions ( $\text{HfC}$  and  $\text{TaC}$ ) and the structure with a Hf:Ta ratio of 50:50 atom % are shown in Figure S5 (Supporting Information). The characteristic feature of all the synthesized powders is a narrow particle size distribution: they have no particles  $>100$  nm. Sometimes nanosized particles are capable to form dense agglomerates caused by their high free surface energy. According to the results of the EDS analysis, the chemical composition of the synthesis products corresponds well with the initial mixtures that were put into the plasma formation channel (Figure S5, Supporting Information). At the same time, there is an obvious excess of carbon, which is due to the work of the graphite electrodes of the magnetoplasma accelerator.

The phase composition and structure of the synthesized powder samples were examined using the X-ray diffraction (Figure S6, Supporting Information). In each product, we identified the formation of a cubic carbide phase (space group  $Fm\bar{3}m$ , no. 225) and a small fraction of unreacted precursors —  $\text{HfO}_2$  and  $\text{Ta}_2\text{O}_5$ . The amount of these impurities varies from fractions of percent to dozens of weight percent. In order to minimize the amount of impurities we performed a series of optimization experiments of synthesis of  $\text{HfTaC}_2$ ,  $\text{Hf}_9\text{TaC}_{10}$ ,  $\text{Hf}_6\text{TaC}_6$ , and  $\text{Hf}_4\text{Ta}_3\text{C}_6$ . Description of these experiments and obtained data is presented in Supporting Information. Dependencies of crystal data of synthesized carbides on the amount of raw carbon in precursor and energy parameters are shown in Tables S8 and S9 (Supporting Information). Evolution of the XRD patterns of synthesized samples with respect to the energy parameters of plasma dynamic synthesis is shown in Figures S8–S11 (Supporting Information).

Obtained information allowed us to obtain the optimal parameters leading to minimization of residual oxide phases. According to obtained data we can conclude that the presence

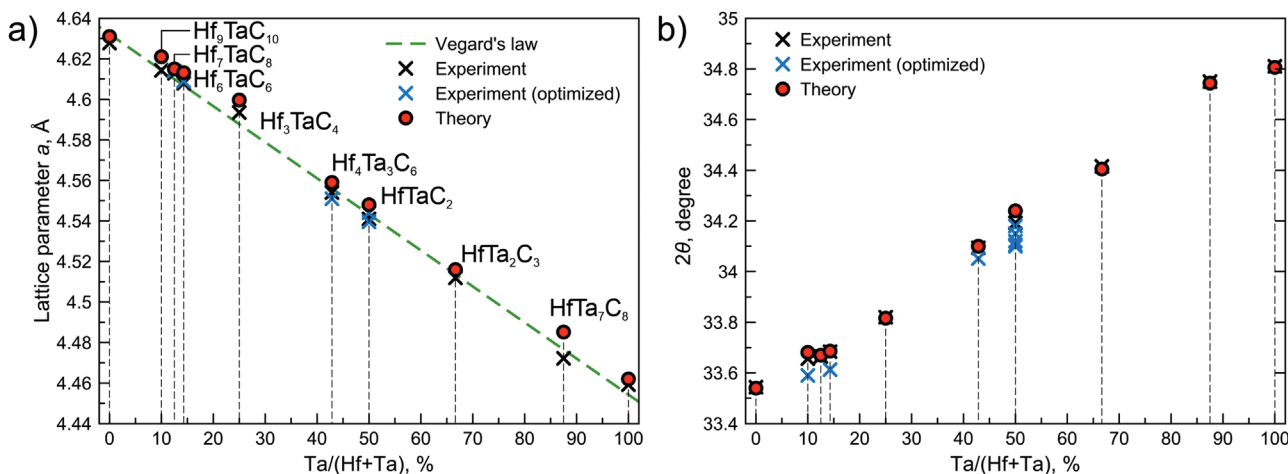


**Figure 2.** Experimental (crosses) and calculated (red circles) a) lattice parameter  $a$  and b)  $2\theta$  diffraction angle of the main (111) reflection of the synthesized Hf–Ta–C compounds. The green dashed line corresponds to Vegard's law. Blue crosses correspond to additional experimental data obtained during the optimization of plasma dynamic parameters (see Supporting Information).

of oxides in the product does not affect the stoichiometry and structure of the synthesized  $\text{Hf}_x\text{Ta}_y\text{C}_z$  powders. From other side, this data shows the high variability of plasma dynamic parameters, which determines the great opportunities for experimental synthesis of various compounds.

Based on the obtained X-ray diffraction patterns, the average values of the lattice constant  $a$  of the synthesized carbide phases were calculated (Table S7, Supporting Information).

We also calculated the lattice parameter and  $2\theta$  angle of the main (111) reflection for all the synthesized compounds (Figure 2). The green dashed line in Figure 2a represents Vegard's law. There is close agreement between the theoretical and experimental data on the lattice parameters (Figure 2a). The lattice parameter decreases as the concentration of Ta in the ternary compound grows. The obtained values unambiguously fit into a linear law. The same behavior was observed for the main (111) reflection, which shifts toward higher angles as the Ta concentration in the compound increases (Figure 2b). The data confirms the efficiency of the proposed approach of selective synthesis of new Hf–Ta–C compounds with a possibility to fine-tune the composition during the process.

Changing the Hf:Ta ratio in the initial powder mixture makes it possible to vary the stoichiometry of the  $\text{Hf}_x\text{Ta}_y\text{C}_z$  compound in a wide range and to finely adjust the crystal structure, in particular the lattice parameter  $a$  in the range from 4.4590 to 4.6277 Å. At the same time, the reference XRD patterns of conventional stoichiometric compounds of cubic HfC (JCPDS card No. 00-039-1491) and TaC (JCPDS card No. 00-035-0801) perfectly correspond to the lattice constants  $a = 4.63765$  and 4.45470 Å, respectively.

Changes in the stoichiometry of ternary  $\text{Hf}_x\text{Ta}_y\text{C}_z$  compounds are probable because of a wide area of homogeneity of the cubic carbide phases in the Hf–Ta–C system: HfC and TaC have the same NaCl-type crystal structure and can form infinite Hf–Ta–C solid solutions in the whole range of compositions.<sup>[23]</sup> The obtained values of the lattice constant  $a$  show that the plasma dynamic synthesis makes it possible to produce not only the well-known HfC, TaC, and  $\text{HfTa}_2\text{C}_2$  compounds,

but also specific and hypothetical  $\text{Hf}_9\text{TaC}_{10}$ ,  $\text{Hf}_7\text{TaC}_8$ ,  $\text{Hf}_6\text{TaC}_6$ ,  $\text{Hf}_3\text{TaC}_4$ ,  $\text{Hf}_4\text{Ta}_3\text{C}_6$ ,  $\text{HfTa}_2\text{C}_3$ , and  $\text{HfTa}_7\text{C}_8$  having a cubic structure.  $\text{Hf}_7\text{TaC}_6$ ,  $\text{Hf}_4\text{Ta}_3\text{C}_6$ ,  $\text{HfTa}_2\text{C}_3$ , and  $\text{HfTa}_7\text{C}_8$  were predicted for the first time, while other compounds have recently been computationally predicted.<sup>[16]</sup>

The structure of the synthesized powders was studied using the transition electron microscopy (TEM) analysis (Figure 3). The bright-field TEM images (Figure 3d–f) of the studied agglomerates of HfC,  $\text{HfTa}_2\text{C}_2$ , and TaC show a set of crystalline particles in a matrix of low-density material. The selected area electron diffraction (SAED) patterns (Figure 3a–c) include an amorphous halo and a set of reflections from the crystal phases forming individual Debye rings and corresponding to the interplanar spacing of HfC,  $\text{HfTa}_2\text{C}_2$ , and TaC.

In general, the microstructure of the obtained products weakly changes depending on the composition and the ratio of precursors. Most synthesized particles form high-contrast polyhedrons with a narrow size distribution (up to 50–70 nm). When the microscope aperture is shifted to the region of point reflections from carbide materials, the reflecting crystal planes give a characteristic bright glow in the dark-field images (Figure 3g–i), which allows the identification of the crystal phases of HfC,  $\text{HfTa}_2\text{C}_2$ , and TaC.

The bright-field images (Figure 3d–f) show dense and contrasting carbide particles surrounded by a crystalline shell of loose material. All these structural units unambiguously correspond to a blurred halo on the SAED patterns with the interplanar spacing corresponding to the set of (002) crystal planes of graphite (Figure 3a–c). Separate carbon objects and the carbon matrix give a characteristic bright glow in the dark-field images when the microscope aperture is shifted to the region of point reflections from carbon (Figure 3j–l). Previously, formation of matrix carbon structures has been correlated with the so-called bound and unbound carbon.<sup>[24]</sup>

The presence of excess carbon seems critical for obtaining a product containing nonstoichiometric carbides of heavy transition metals because it requires formation of structures from the shell carbide particles.<sup>[25]</sup> The results of the detailed

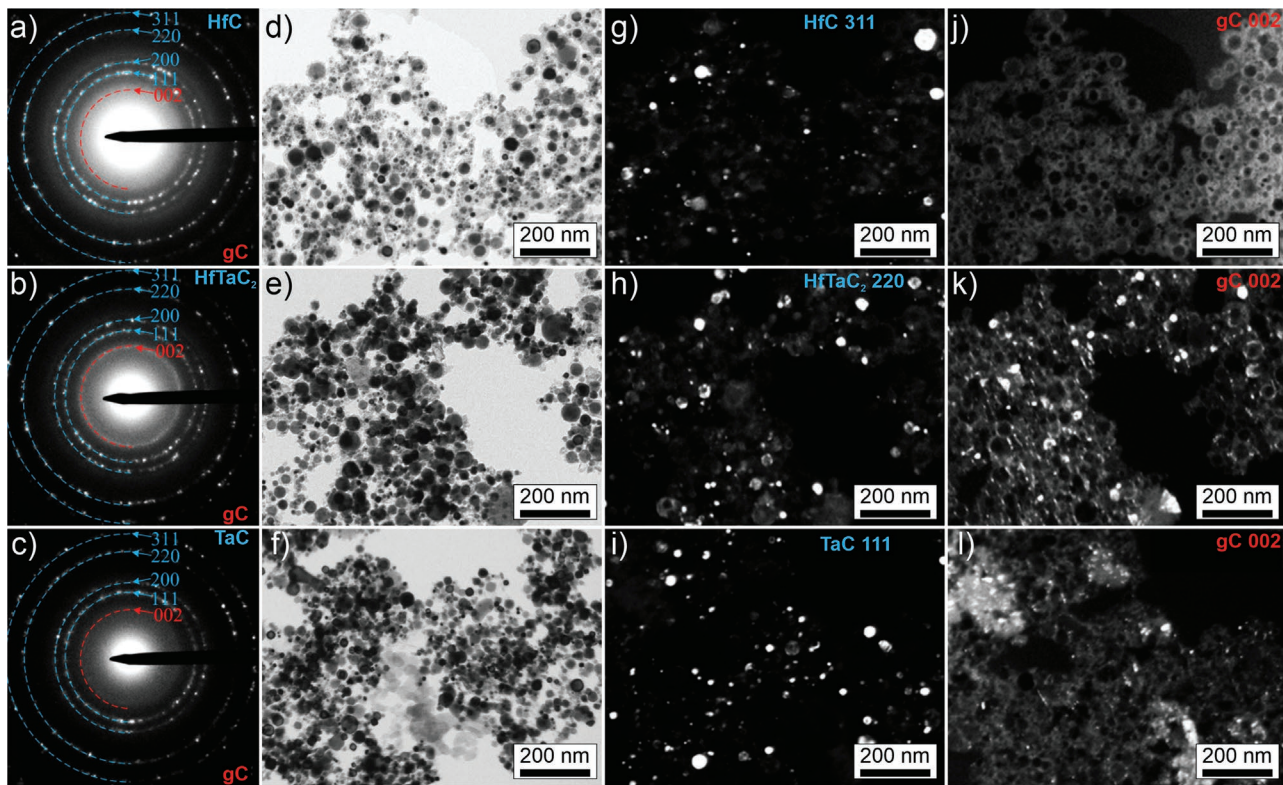


**Figure 3.** Transmission electron microscopy analysis of the synthesized HfC, HfTaC<sub>2</sub>, and TaC samples: a–c) SAED, d–f) bright-field TEM images. Dark-field TEM images with an aperture shifts to the region of reflections corresponding to the g–i) carbide and j–l) graphite phases.

high-resolution TEM study of the obtained carbide particles are shown in Figure S7 (Supporting Information). All particles show high crystallinity with a clearly observed cubic structure.

The critical condition for the synthesis of nonstoichiometric Hf<sub>x</sub>Ta<sub>y</sub>C<sub>z</sub> compounds is a high rate of crystallization, which has been previously confirmed by Shanenkov et al.<sup>[26]</sup> for nonstoichiometric metastable carbide WC<sub>1-x</sub>. We chose a copper substrate for the synthesis of coatings of the predicted Hf-Ta-C compounds because copper has a high thermal conductivity of 395 W m<sup>-1</sup> K<sup>-1</sup>. The mass and atomic ratios of Hf and Ta in the oxide composition of the initial mixture of precursors for the synthesis of the predicted nonstoichiometric coatings are shown in Table S2 (Supporting Information), the XRD patterns of the synthesized coatings — in Figure S12 (Supporting Information). All the XRD patterns show reflections at  $2\theta = 43.32^\circ$ ,  $50.45^\circ$ ,  $74.13^\circ$ , and  $89.94^\circ$ , which correspond to the copper substrate and are excluded from the analysis. The ratio of the intensities of the main reflections of the copper substrate to those of the Hf-Ta-C coating indicates a small thickness or heterogeneity of the coating, which transmits a significant part of the X-ray radiation. High-intensity reflections indicate the presence of the cubic carbide phase with  $Fm\bar{3}m$  space group symmetry.

The unambiguous change in the structure of the formed phases comes from the dependence of the lattice parameter  $a$  and the  $2\theta$  position of the main (111) X-ray reflection on the composition of the coating (Figure 4a). The average values of the lattice parameter  $a$  change linearly from 4.4578 to 4.6292 Å with increasing Ta content in the precursor mixture, which fully corresponds with both the theoretical dependence obtained

from Vegard's law (green dashed line in Figure 4a) and the DFT-calculated values (black circles in Figure 4a). The calculated average lattice parameter values are presented in Table S11 (Supporting Information).

Thus, the plasma dynamic synthesis can be considered a universal method for obtaining a wide range of nonstoichiometric Hf-Ta-C compounds both in the bulk and dispersed forms. In the case of coatings, the possibility of forming nonstoichiometric compounds having a cubic structure and the HfTaC<sub>2</sub>, Hf<sub>3</sub>TaC<sub>4</sub>, and HfTa<sub>2</sub>C<sub>3</sub> composition is shown directly.

For the obtained coatings (HfC, TaC, Hf<sub>3</sub>TaC<sub>4</sub>, HfTaC<sub>2</sub>, and HfTa<sub>2</sub>C<sub>3</sub>), the SEM images of both surfaces and cross sections were measured as shown in Figure 4b–k. The surfaces of all the coatings are quite rough and heterogeneous, with noticeable formation of individual grains up to several microns in size.

The cross-sectional SEM images of the synthesized material show a heterogeneous structure with a clearly identified interface between the coating and substrate. The coating has no intermediate layers of the substrate melt. This is similar to nonstoichiometric WC<sub>1-x</sub> coatings obtained using the plasma dynamic synthesis.<sup>[26]</sup> The thickness of the synthesized Hf-Ta-C coatings is from 2 to 10 µm. The coatings formed as either a relatively homogeneous solid layer (Figure 4c,e,g) or several superimposed layers (Figure 4i,k), some of them have individual grains of material up to 1 µm in size (Figure 4k).

It has been noted before that the plasma dynamic method has a high crystallization rate of  $\approx 10^8$ – $10^{11}$  K s<sup>-1</sup>. Although this seems to have a positive effect on the composition of the synthesized product, the abrupt cooling nevertheless leads to negative

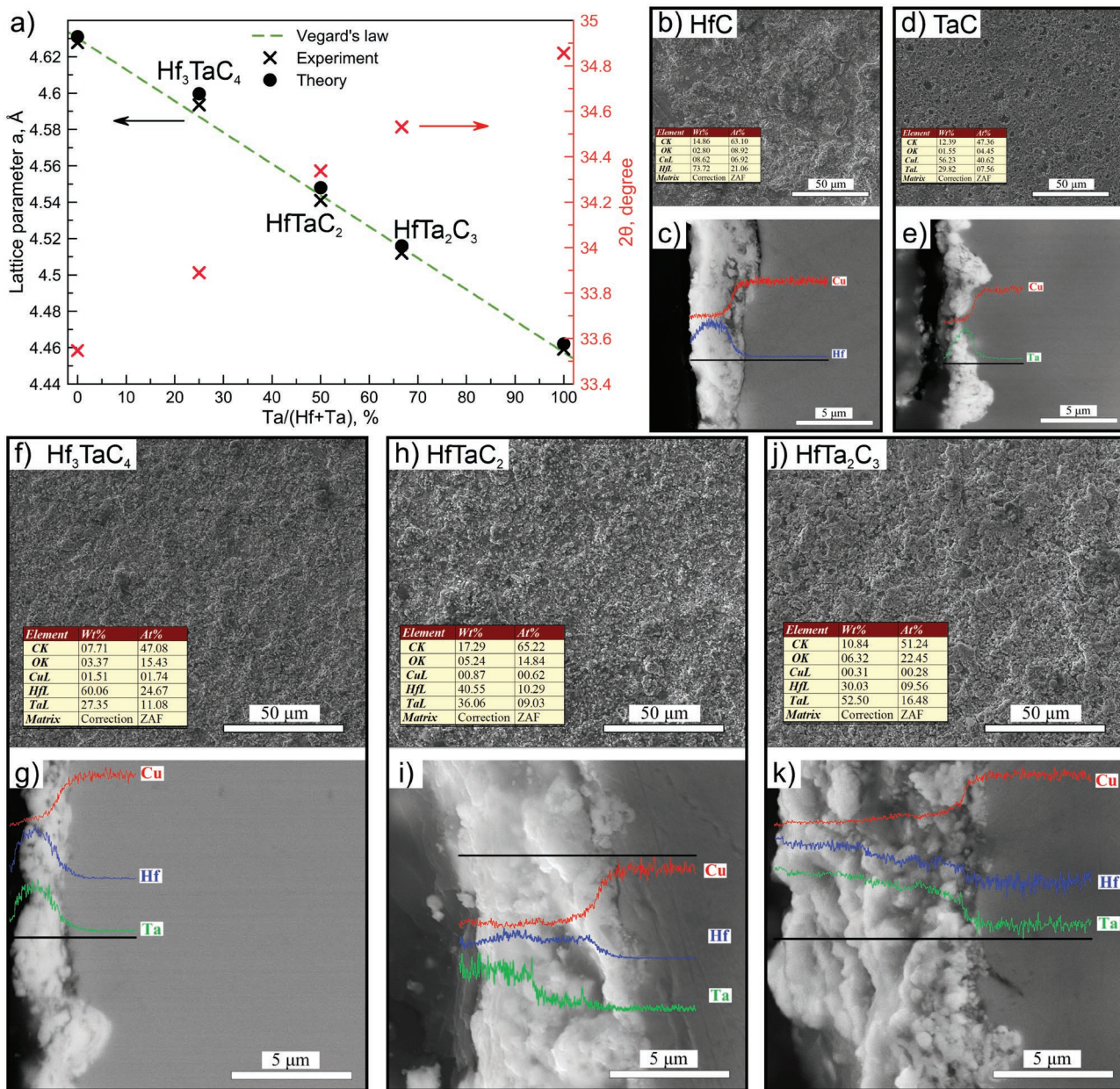


**Figure 4.** a) Experimental (black crosses) and calculated (black circles) lattice parameter  $a$  and the position of the main (111) XRD reflection (red crosses) of the synthesized coatings. SEM images and EDS analysis of the synthesized coatings: b,c) HfC, d,e) TaC, f,g) Hf<sub>3</sub>TaC<sub>4</sub>, h,i) HfTaC<sub>2</sub>, and j,k) HfTa<sub>2</sub>C<sub>3</sub>.

consequences for the structure of the coating material. Whereas generally the coating is tightly bonded to the substrate, cracks between them still form naturally under conditions of high-power sputtering of coatings in plasma methods.<sup>[27]</sup> Another factor is a significant difference in the thermal properties of the coating and the substrate,<sup>[28]</sup> which leads to formation of cracks between them during intense heating and cooling caused by tangential stresses.

The results of the EDS analysis — the content curves of the elements Hf, Ta, and Cu — show the formation of a coating structure containing compounds based on Hf or Ta, or both, deposited on a copper substrate. For the Hf–Ta–C ternary

system, the EDS curves of Hf and Ta have a similar behavior, which indicates the formation of Hf<sub>x</sub>Ta<sub>y</sub>C<sub>z</sub>-type compounds rather than the synthesis of separate phases of hafnium and tantalum carbides. The formation of such ternary carbides is promoted by a high cooling rate during crystallization. Carbides are formed in the interaction of a supersonic high-temperature plasma ( $\approx 10\ 000$  K), which contains hafnium, tantalum, and carbon in a liquid phase, with the surface of a copper substrate. The hafnium–tantalum–carbon melt crystallizes in the conditions of high-intensity heat removal by the copper substrate at 3942–3980 °C, according to the phase diagrams of the Hf–C and Ta–C systems.<sup>[29]</sup> The adhesion of the coating to the

substrate is achieved by partial melting of the copper substrate to a very limited depth.

The synthesis of the bulk Hf–Ta–C material allowed us to directly measure the mechanical properties of nonstoichiometric carbides for the first time using the nanoindentation method. Because of difficulties in measuring the hardness of thin Hf–Ta–C films, we made measurements only for the thickest coating, HfTa<sub>2</sub>C<sub>3</sub>. The load–unload curves (Figure S13, Supporting Information) show the maximum achieved displacement of 140 nm at the load of 5 mN, whereas the final depth was 60 nm. The obtained values of nanohardness  $H_V = 16.2 \pm 3.5$  GPa and Young's modulus  $E = 167.8 \pm 25.0$  GPa. The large standard deviations of the values are associated with heterogeneity of the coating, the presence of pores and structural defects.<sup>[23]</sup> However, the obtained values are sufficiently larger than the hardness of the copper substrate  $H_V = 1.4$  GPa. The obtained nanohardness of the HfTa<sub>2</sub>C<sub>3</sub> coating is comparable with the hardness of pure hafnium and tantalum carbides (11–15 GPa<sup>[30,31]</sup>) and of HfTaC<sub>2</sub>, which equals 20–28 GPa.<sup>[23,30]</sup>

High values of hardness of the synthesized coatings result from the reaction of TaC with HfC in the solution that involves the mutual substitution of the Hf and Ta atoms in the crystal lattice, which is similar to the mechanism of solid solution hardening in alloys.<sup>[32]</sup> Formation of a hard coating makes it possible to harden metal substrate surfaces and increase their wear resistance.

Thus, the plasma dynamic synthesis technique allows us to obtain Hf<sub>x</sub>Ta<sub>y</sub>C<sub>z</sub> bulk nonstoichiometric compounds. The synthesized coatings correspond to cubic bulk phases of HfC, Hf<sub>3</sub>TaC<sub>4</sub>, HfTaC<sub>2</sub>, HfTa<sub>2</sub>C<sub>3</sub>, and TaC, depending on the Hf:Ta

ratio in the initial raw powder. Formation of cracks in the coatings and their small thickness require further optimization of the plasma dynamic technique toward the synthesis of denser and thicker coatings with subsequent study of the tribological and adhesion properties. However, despite these disadvantages, the synthesis of nonstoichiometric ternary carbides is unique, having no analogues in the world. For the first time, direct measurements of the physical and mechanical properties of these materials were made, showing sufficiently high nanohardness and Young's modulus and a possibility of using them to harden metal substrates.

To study the thermal properties and thermal stability of the synthesized Hf–Ta–C compounds, we performed direct annealing of the samples of HfC, TaC, and HfTaC<sub>2</sub>. The XRD patterns at various temperatures show changes in the composition during annealing (Figures S14–S16, Supporting Information). The oxidation of each studied material starts from 500 °C with the formation of metal oxides. The detailed description of phase transformations is presented in Supporting Information.

The observed features in the behavior of these materials during the oxidation are consistent with the data of the differential thermal analysis, which was performed for the samples of HfC, Hf<sub>3</sub>TaC<sub>4</sub>, HfTaC<sub>2</sub>, HfTa<sub>2</sub>C<sub>3</sub>, and TaC (Table S12, Supporting Information). The results of the TG, DTG, DSC, and mass spectrometry are shown in Figure 5. The TF and DTG curves (Figure 5a,b) show that the mass of the studied samples changes in a three-step manner during the heating.

In the first stage, a monotonic weight reduction up to 200 °C is observed, which is caused by the removal of the adsorbed moisture from the surface of nanoparticles. This process is

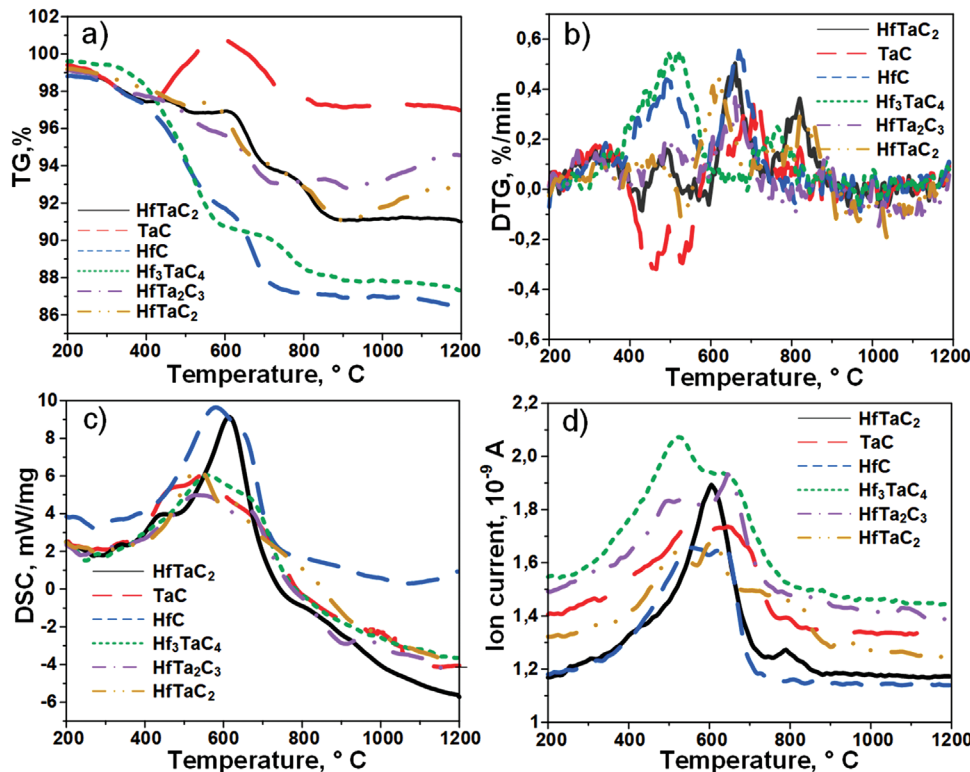


Figure 5. Thermal analysis of the synthesized Hf–Ta–C compounds: a) TG, b) DTG, c) DSC, and d) mass spectrometry (MS) for CO<sub>2</sub> gas ( $m/z = 44$ ).

confirmed by the XRD data (Figures S14–S16, Supporting Information). In the second stage, there is a gain of mass in the temperature range of 400–600 °C, caused by intense oxidation.<sup>[33]</sup> The third stage shows a decrease of several percent in the material mass in the temperature range from 600 to 800 °C due to the possible oxidation of unbound carbon with the formation of carbon dioxide CO<sub>2</sub>. A decrease in the mass of some of the studied samples starts from ≈300 °C, which may also result from the oxidation of carbon structures, in particular graphite.<sup>[34]</sup>

Contrasting behavior of the TG and DTG curves of the TaC sample showing a larger mass gain during oxidation is caused by a higher oxygen content in Ta<sub>2</sub>O<sub>5</sub> compared to HfO<sub>2</sub>. In general, an increase in the hafnium content leads to a sharper mass decrease and less noticeable mass gain section. The temperature of the maximum oxidation reaction rate  $T_{\max}$  for the Hf–Ta–C samples varied in the range of 530–660 °C. The position of the exothermic maximum on the DSC curves (Figure 5c) is comparable to the  $T_{\max}$  values. The observed exothermic effects were associated with the heat release during the oxidation of carbon. As the amount of carbon in the samples increased, the calculated value of the subintegral area of the DSC curves also rose. The MS curves for CO<sub>2</sub> gas ( $m/z = 44$ ) include peaks at 370 °C (Figure 5d) and correspond to CO<sub>2</sub> released due to the reaction of carbon with oxygen. This reaction continues up to 800 °C leading to a continuous reduction in the mass of the material.

The application of the plasma dynamic technique for the synthesis of Hf–Ta–C compounds results in formation of both high-quality powders and protective coatings composed of nonstoichiometric hafnium–tantalum carbides. The implications and importance of this work extend far beyond the results shown herein: It is possible to construct >70 combinations of group 4 and 5 transition metals in ternary and quaternary carbides, and this research opens the door for formation of a large number of new materials including carbides and, possibly, borides of Ti, Zr, Hf, V, Nb, and Ta. Materials and coatings based on carbides of these elements can be selectively synthesized if the plasma dynamic synthesis is extended to other multicomponent transition metal carbides and borides

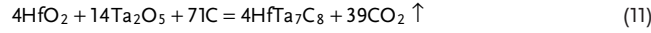
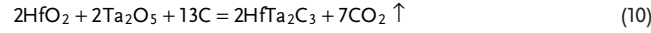
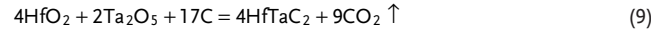
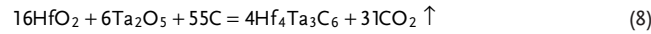
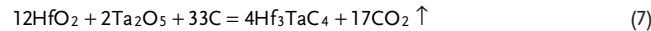
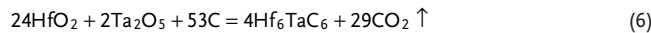
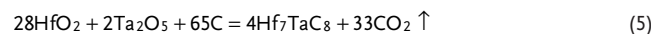
### 3. Experimental Section

**Experimental Details:** Powders and coatings in the Hf–Ta–C system were synthesized using the plasma dynamic method, which was based on the high-energy pulsed electric discharge plasma flow generated by a pulsed high-current coaxial magnetic plasma accelerator. The plasma accelerator was a system of coaxially arranged graphite electrodes placed in an external induction system and rigidly fixed related to each other. Pulse electric power supply of the plasma accelerator from a capacitive energy storage device ( $C = 6.0$  mF,  $U = 3.0$  kV) produces an arc discharge with the current amplitude  $I \approx 100$  kA and maximum power  $P \approx 120$  MW. The plasma flow streams into a hermetically sealed reactor filled with argon at a pressure of 1 atm. The principle of operation and the design of the plasma dynamic synthesis system had been discussed in detail previously for producing powders<sup>[35–37]</sup> and coatings<sup>[26]</sup> of various metal carbides.

For the synthesis of Hf–Ta–C coatings, a different reactor chamber with a volume  $V = 0.054$  m<sup>3</sup> ( $d = 260$  mm;  $l = 980$  mm) was used. In the chamber, a copper plate substrate (50 × 50 × 3 mm) was set at 65 mm from the plasma accelerator edge, the distance that had been

experimentally established<sup>[26]</sup> in terms of optimal interaction with the plasma. A more detailed description can be found in Supporting Information, with the typical oscilloscopes (Figure S3, Supporting Information) and energy parameters (Table S3, Supporting Information).

The powders of crystalline hafnium (IV) oxide HfO<sub>2</sub> (grade HfO-1, 99.9%, Rare Metal, Russia) and tantalum (V) oxide Ta<sub>2</sub>O<sub>5</sub> (purity of 99.99%, Rare Metal, Russia) and amorphous technical carbon (99.0%, Chemical Department of Tomsk Polytechnic University, Russia) were used as precursors in the synthesis. The possibility of obtaining dispersed and bulk (in the form of coatings) Hf<sub>x</sub>Ta<sub>y</sub>C<sub>z</sub> materials in a wide stoichiometric range from pure HfC to TaC is investigated. The mass and atomic ratios of Hf and Ta in the initial oxide compounds in the powder mixture are shown in Table S1 (Supporting Information). To correctly define the mass and atomic ratios of the precursors, the following chemical reactions were considered:



The precursors were mixed for 10 h using a SPEX Sample Prep. Mixer/Mill 8000 M in a ZrO<sub>2</sub> milling vessel with two balls of the same material for additional particle size reduction and mechanical activation. The mixture was then injected axially into the plasma formation channel, which was a cylinder with a diameter of 7 mm and a height of 10 mm. The information on the phase composition and microstructure of the initial powder mixtures used as precursors is presented in Figures S1 and S2 (Supporting Information).

The resulting powders were collected from the reactor chamber. The X-ray phase analysis was carried out using Shimadzu XRD 7000 X-ray diffractometer (CuK $\alpha$ -irradiation with graphite monochromator with  $\lambda = 1.5406$  Å) within the angle range  $2\theta$  from 10 to 90°. The identification of the diffraction reflections was carried out using the PDF4+ database and Crystallographica Search Match software. The average value of the lattice constant  $a$  of cubic nonstoichiometric Hf<sub>x</sub>Ta<sub>y</sub>C<sub>z</sub> compounds was determined by the positions of the X-ray maximums  $2\theta_{hkl}$  with the Miller indices (111), (200), (220), (311), (222), (400) and the corresponding interplanar spacing  $d_{hkl}$ .

To determine the position of the X-ray maximum of coatings more accurately, an X-ray imaging of the samples was carried out according to the asymmetric geometry in the sliding beam mode with a fixed beam angle from the X-ray source  $\theta_1 = 3^\circ$  and a varying detector angle  $\theta_2 = 10\text{--}90^\circ$ .

Quanta 200 3D scanning electron microscope (SEM) with an energy dispersive spectroscopy (EDS) attachment was used to study the structure and elemental composition of the disperse product and coatings. The transmission electron microscopy (TEM) analysis was performed using Phillips CM 12 microscope and JEOL JEM 2100F high-resolution microscope (HRTEM) to investigate the morphology and size of nanoparticles in the synthesized powders. The high-resolution images were processed using Gatan 1.80.70 software package.

The thermal stability of the products obtained by the plasma dynamic synthesis was investigated using both the differential thermal analysis (DTA) and direct annealing methods. The first method was implemented using Netzsch STA 449 F3 Jupiter simultaneous thermal analyzer with the ability to measure mass changes, thermal effects, and ion currents of different gases. Using the thermogravimetry (TG, DTG), differential scanning calorimetry (DSC), and mass spectrometry (MS) methods, the corresponding curves were plotted. The DTG studies were performed in  $\text{Al}_2\text{O}_3$  cuvettes at a heating rate of  $10\text{ }^\circ\text{C min}^{-1}$  in air.

The direct annealing of the dispersed product was performed in mullite cuvettes in P310 Nabertherm atmospheric furnace at a heating rate of  $10\text{ }^\circ\text{C min}^{-1}$ . The holding time at the required maximum temperature was 1 h, after which the powder was naturally cooled. After annealing to 400, 600, 800, and  $1000\text{ }^\circ\text{C}$ , the material was studied using the X-ray diffraction (XRD) and transmission electron microscopy.

To study the composition and structure of the synthesized coatings, an area of  $\approx 10\text{ mm}^2$  was cut out in each coating using a cutting machine. The obtained samples were placed in separate casting molds, where a special casting compound Technovit 5000 was poured. After hardening, a full cycle of metallographic preparation was carried out for the subsequent study of the surface microstructure of the coating section. The obtained samples were polished, first with grinding disks of SiC 320, 600, 800, and 1200, then with polishing cloths of 6, 3, 1, and 0,25 microns and corresponding diamond suspensions and greasing on a polishing-grinding machine Forcipol 1 V. Direct cross-sectional images of the coatings were obtained using Quanta 3D scanning electron microscope system and studied in terms of elemental composition using the EDS analysis.

The mechanical characteristics of the coatings were studied using Table Top Nanoindentation Tester (TTX-NHT) based on the Berkowitz method with a load of 5 mN and a loading rate of  $10\text{ mN min}^{-1}$  according to the common methodology (ASTM C1327-15 (2019)). The nanohardness values and elastic modulus of a  $\text{Ta}_x\text{Hf}_y\text{C}_z$  coating can be obtained from the load–displacement curve using the Oliver–Pharr method.<sup>[38]</sup>

**Computational Details:** The prediction of stable crystal structures in the ternary Hf–Ta–C system was carried out using the variable-composition evolutionary algorithm USPEX.<sup>[39–41]</sup> Because of the large compositional and configurational space of search, we used a previously proposed multistep procedure of prediction<sup>[42]</sup> consisting of: i) the collection of all possible information about binary compounds (the edges of a triangular phase diagram) from literature and a variable-composition evolutionary search for binary compounds (Hf–C, Ta–C, Hf–Ta); ii) a variable-composition evolutionary search for ternary compounds, without any restrictions except for the number of atoms in the unit cell ( $\leq 48$  atoms); iii) a variable-composition evolutionary search for ternary compounds with seeds that consist of all known unary, binary, and ternary compounds; and iv) an evolutionary search along the pseudobinary joints determined from steps (ii) and (iii). Step (i) enabled the prediction of all structures of binary compounds necessary for step (iii), whereas step (ii) made it possible to find all stable and metastable structures of ternary compounds that do not have the same crystal structure types as binary compounds.

During the structure search, the first generation of 300 structures was produced randomly with up to 48 atoms in the primitive cell. Each subsequent generation consisting of 200 structures was produced by applying the heredity (40% of each generation), softmutation (20%), and transmutation (20%) operators; 20% of each generation was produced using random symmetric<sup>[41]</sup> and random topological generators.<sup>[43]</sup> Additional searches for stable structures were performed for the HfTa–C, HfC–TaC, and HfC–Ta<sub>2</sub>C systems, where the first generation of the structure candidates contained 150 structures with up to 48 atoms in the primitive cell; succeeding generations contained 100 structures.

Our calculations were based on the density functional theory (DFT)<sup>[44,45]</sup> within the generalized gradient approximation (the Perdew–Burke–Ernzerhof functional)<sup>[46]</sup> and the projector augmented wave method<sup>[47,48]</sup> as implemented in the VASP<sup>[49–51]</sup> code. The plane wave energy cutoff of 500 eV, the Methfessel–Paxton smearing<sup>[52]</sup> of electronic occupations, and  $\Gamma$ -centered  $k$ -point meshes with a resolution of

$2\pi \times 0.015\text{ \AA}^{-1}$  for the Brillouin zone sampling were used, ensuring the convergence of the energy differences and stress tensors.

Stability at finite temperatures was studied by calculating the Helmholtz free energy as follows:

$$F(T) = E_0(V) + F_{\text{vib}}(V, T) + TS_{\text{conf}} \quad (13)$$

where  $E_0$  is the total energy from the DFT calculations,  $TS_{\text{conf}}$  is the contribution associated with the configurational entropy,  $F_{\text{vib}}$  is the vibrational Helmholtz free energy calculated from the following relation in the harmonic approximation:<sup>[53]</sup>

$$F_{\text{vib}}(V, T) = k_B T \int_{\Omega} g(\omega(V)) \ln \left[ 1 - \exp \left( -\frac{\hbar \omega(V)}{k_B T} \right) \right] d\omega + \frac{1}{2} \int_{\Omega} g(\omega(V)) \hbar \omega d\omega \quad (14)$$

Here  $g(\omega(V))$  is the phonon density of states at a given volume, calculated using the finite displacements method as implemented in PHONOPY,<sup>[54,55]</sup> with forces computed using VASP<sup>[49–51]</sup>.

## Supporting Information

Supporting Information is available from the Wiley Online Library or from the author.

## Acknowledgements

A.G.K. and I.V.C. thank the Russian Science Foundation (№ 19-72-30043). The calculations were carried out on Arkuda supercomputer of the Skolkovo Foundation. The high-resolution microscopy research was carried out using the equipment of the Center for Collective Use “Nanomaterials and Nanotechnologies” of Tomsk Polytechnic University supported by the RF Ministry of Education and Science project #075-15-2021-710. The experimental research was supported by the TPU development program. The authors also thank Igor Grishin (Skoltech) for proofreading the manuscript.

## Conflict of Interest

The authors declare no conflict of interest.

## Authors Contribution

A.G.K. and D.S.N. contributed equally to this work. A.G.K. and A.Y.P. conceived this project. A.A.S. provided general idea of plasma dynamic method. I.I.S. performed a series of experiments on the synthesis of powders. D.S.N. performed all experiments with coatings, microscopy analysis, and hardness measurements. A.Y.P. made X-ray diffraction analysis during whole study. Z.B. carried out thermal analysis of obtained powders. A.N. did experiments on a pulsed accelerator for the synthesis of tantalum–hafnium carbide. A.G.K. performed computational prediction of stable structures, I.V.C. and Y.A.K. performed calculations of phonons and construction of high-temperature diagrams. A.G.K. prepared the analysis of results and wrote the manuscript. All the authors provided critical feedback and helped shape the research.

## Data Availability Statement

The data that support the findings of this study are available in the supplementary material of this article.

## Keywords

computational discovery, hafnium-tantalum carbides, nonstoichiometric compounds, plasma dynamic synthesis, protective coatings

Received: June 2, 2022  
Published online:

- [1] E. Wuchina, E. Opila, M. Opeka, B. Fahrenholtz, I. Talmi, *Electrochem. Soc. Interface* **2007**, 16, 30.
- [2] L. Toth, *Transition Metal Carbides and Nitrides*, Elsevier, Cham, Switzerland **2014**.
- [3] D. J. Rowcliffe, in *Deformation of Ceramic Materials II* (Eds: R. E. Tressler, R. C. Bradt), Springer US, Boston, MA, **1984**, pp. 49–71.
- [4] D. J. Green, *An Introduction to the Mechanical Properties of Ceramics*, Cambridge University Press, Cambridge, UK **1998**.
- [5] D. R. Lide (Ed.), *Handbook of Chemistry and Physics*, 81st ed., CRC Press, Boca Raton, **2000**.
- [6] E. Castle, T. Csanádi, S. Grasso, J. Dusza, M. Reece, *Sci. Rep.* **2018**, 8, 8609.
- [7] X.-X. Yu, G. B. Thompson, C. R. Weinberger, *J. Eur. Ceram. Soc.* **2015**, 35, 95.
- [8] O. Cedillos-Barraza, S. Grasso, N. A. Nasiri, D. D. Jayaseelan, M. J. Reece, W. E. Lee, *J. Eur. Ceram. Soc.* **2016**, 36, 1539.
- [9] Q.-J. Hong, A. van de Walle, *Phys. Rev. B* **2015**, 92, 020104.
- [10] C. Zhang, A. Gupta, S. Seal, B. Boesl, A. Agarwal, *J. Am. Ceram. Soc.* **2017**, 100, 1853.
- [11] R. A. Andrievskii, N. S. Strel'nikova, N. I. Poltoratskii, E. D. Kharkhardin, V. S. Smirnov, *Porosh. Met., Akad. Nauk Ukr. SSR* **1967**, 1, 85.
- [12] C. Agte, H. Alterthum, *Z. Tech. Phys.* **1930**, 11, 182.
- [13] O. Cedillos-Barraza, D. Manara, K. Boboridis, T. Watkins, S. Grasso, D. D. Jayaseelan, R. J. M. Konings, M. J. Reece, W. E. Lee, *Sci. Rep.* **2016**, 6, 37962.
- [14] S. A. Ghaffari, M. A. Faghihi-Sani, F. Golestan-Fard, H. Mandal, *J. Eur. Ceram. Soc.* **2013**, 33, 1479.
- [15] C. J. Smith, X.-X. Yu, Q. Guo, C. R. Weinberger, G. B. Thompson, *Acta Mater.* **2018**, 145, 142.
- [16] X. Liu, H. Niu, A. R. Oganov, *npj Comput. Mater.* **2021**, 7, 199.
- [17] S.-K. Sun, G.-J. Zhang, W.-W. Wu, J.-X. Liu, T. Suzuki, Y. Sakka, *Scr. Mater.* **2013**, 69, 139.
- [18] A. Sedegov, S. Vorotilo, V. Tsybulin, K. Kuskov, D. Moscovskikh, *IOP Conf. Ser.: Mater. Sci. Eng.* **2019**, 558, 012043.
- [19] P. Zhang, X. Liu, A. Cai, Q. Du, X. Yuan, H. Wang, Y. Wu, S. Jiang, Z. Lu, *Sci. China Mater.* **2021**, 64, 2037.
- [20] K. Sun, Z. Yang, R. Mu, S. Niu, Y. Wang, D. Wang, *J. Eur. Ceram. Soc.* **2021**, 41, 3196.
- [21] L. Feng, W. G. Fahrenholtz, G. E. Hilmas, *J. Am. Ceram. Soc.* **2019**, 102, 7217.
- [22] A. de Monteynard, H. Luo, M. Chehimi, J. Ghanbaja, S. Achache, M. François, A. Billard, F. Sanchette, *Coatings* **2020**, 10, 212.
- [23] Z. Y. Tan, W. Zhu, L. Yang, Y. C. Zhou, Q. Wu, L. J. Gong, *Surf. Coat. Technol.* **2020**, 403, 126405.
- [24] I. Shanenkov, A. Ivashutenko, Y. Shanenkova, D. Nikitin, Y. Zhu, J. Li, W. Han, A. Sivkov, *J. Alloys Compd.* **2020**, 834, 155116.
- [25] I. Shanenkov, D. Nikitin, A. Ivashutenko, Y. Shanenkova, Y. Vympina, D. Butenko, W. Han, A. Sivkov, *Ceram. Int.* **2021**, 47, 6884.
- [26] I. Shanenkov, D. Nikitin, A. Ivashutenko, I. Rahmatullin, Y. Shanenkova, A. Nassyrbayev, W. Han, A. Sivkov, *Surf. Coat. Technol.* **2020**, 389, 125639.
- [27] M. J. Liu, M. Zhang, X. F. Zhang, G. R. Li, Q. Zhang, C. X. Li, C. J. Li, G. J. Yang, *Appl. Surf. Sci.* **2019**, 486, 80.
- [28] X. Zhang, C. Wang, R. Ye, C. Deng, X. Liang, Z. Deng, S. Niu, J. Song, G. Liu, M. Liu, K. Zhou, J. Lu, J. Feng, *J. Materomics* **2020**, 6, 102.
- [29] Y. Pan, P. Zhou, Y. Peng, Y. Du, F. Luo, *Calphad* **2016**, 53, 1.
- [30] S. Vorotilo, K. Sidnov, A. S. Sedegov, M. Abedi, K. Vorotilo, D. O. Moskovskikh, *Comput. Mater. Sci.* **2022**, 201, 110869.
- [31] F. Rezaei, M. G. Kakroudi, V. Shahedifar, N. P. Vafa, *Ceram. Int.* **2017**, 43, 15537.
- [32] J. Jiang, S. Wang, W. Li, L. Klein, *J. Am. Ceram. Soc.* **2016**, 99, 3198.
- [33] J. Polonský, I. M. Petrushina, E. Christensen, K. Bouzek, C. B. Prag, J. E. T. Andersen, N. J. Bjerrum, *Int. J. Hydrogen Energy* **2012**, 37, 2173.
- [34] N. S. Alhajri, H. Yoshida, D. H. Anjum, A. T. Garcia-Esparza, J. Kubota, K. Domen, K. Takanabe, *J. Mater. Chem. A* **2013**, 1, 12606.
- [35] A. Sivkov, D. Nikitin, I. Shanenkov, A. Ivashutenko, I. Rahmatullin, A. Nassyrbayev, *Int. J. Refract. Met. Hard Mater.* **2019**, 79, 123.
- [36] A. Sivkov, I. Rakhamatullin, I. Shanenkov, Y. Shanenkova, *Int. J. Refract. Met. Hard Mater.* **2019**, 78, 85.
- [37] A. Pak, A. Sivkov, I. Shanenkov, I. Rahmatullin, K. Shatrova, *Int. J. Refract. Met. Hard Mater.* **2015**, 48, 51.
- [38] W. C. Oliver, G. M. Pharr, *J. Mater. Res.* **1992**, 7, 1564.
- [39] A. R. Oganov, C. W. Glass, *J. Chem. Phys.* **2006**, 124, 244704.
- [40] A. R. Oganov, A. O. Lyakhov, M. Valle, *Acc. Chem. Res.* **2011**, 44, 227.
- [41] A. O. Lyakhov, A. R. Oganov, H. T. Stokes, Q. Zhu, *Comput. Phys. Commun.* **2013**, 184, 1172.
- [42] A. G. Kvashnin, C. Tantardini, H. A. Zakaryan, Y. A. Kvashnina, A. R. Oganov, *Chem. Mater.* **2020**, 32, 7028.
- [43] P. V. Bushlanov, V. A. Blatov, A. R. Oganov, *Comput. Phys. Commun.* **2019**, 236, 1.
- [44] P. Hohenberg, W. Kohn, *Phys. Rev.* **1964**, 136, B864.
- [45] W. Kohn, L. J. Sham, *Phys. Rev.* **1965**, 140, A1133.
- [46] J. P. Perdew, K. Burke, M. Ernzerhof, *Phys. Rev. Lett.* **1996**, 77, 3865.
- [47] P. E. Blöchl, *Phys. Rev. B* **1994**, 50, 17953.
- [48] G. Kresse, D. Joubert, *Phys. Rev. B* **1999**, 59, 1758.
- [49] G. Kresse, J. Hafner, *Phys. Rev. B* **1993**, 47, 558.
- [50] G. Kresse, J. Hafner, *Phys. Rev. B* **1994**, 49, 14251.
- [51] G. Kresse, J. Furthmüller, *Phys. Rev. B* **1996**, 54, 11169.
- [52] M. Methfessel, A. T. Paxton, *Phys. Rev. B* **1989**, 40, 3616.
- [53] G. Kern, G. Kresse, J. Hafner, *Phys. Rev. B* **1999**, 59, 8551.
- [54] A. Togo, I. Tanaka, *Scr. Mater.* **2015**, 108, 1.
- [55] A. Togo, F. Oba, I. Tanaka, *Phys. Rev. B* **2008**, 78, 134106.